

Bond behaviour improvement between infra-lightweight and high strength concretes using FRP grid reinforcements and development of bond strength prediction models

Yue Liu^a, T. Tafsirojjaman^{b,e*}, Attiq Ur Rahman Dogar^c, Alexander Hückler^d

^a The Key Laboratory of Urban Security and Disaster Engineering of Ministry of Education, Beijing University of Technology, 100 Pingleyuan, Beijing, China

^b School of Civil and Environmental Engineering, Faculty of Science and Engineering, Queensland University of Technology, 2 George Street, Brisbane, QLD 4000, Australia.

^c Department of Civil Engineering, University of Central Punjab, Lahore, Pakistan.

^d Chair of Conceptual and Structural Design, Institute of Civil Engineering, Technische Universität Berlin, Berlin, Germany.

^e Centre for Future Materials (CFM), School of Civil Engineering and Surveying, University of Southern Queensland, Toowoomba, QLD, 4350, Australia.

(*Corresponding author: tafsirojjaman@hdr.qut.edu.au (T. Tafsirojjaman)

Email addresses: yliu@bjut.edu.cn (Yue Liu), tafsirojjaman@hdr.qut.edu.au (T. Tafsirojjaman), attiq.dogar@ucp.edu.pk (Attiq Ur Rahman Dogar), alexander.hueckler@tu-berlin.de (Alexander Hückler).

Abstract

The structural performance of a newly developed lightweight and thermally efficient alternate of normal concrete (NC) i.e. infra-lightweight concrete (ILC) had been under question due to its low elastic modulus, surface roughness, and cracking. In the present study, the structural performance of ILC has been improved by using a layer of high strength concrete (HSC) on each side of the ILC. As the efficiency of the ILC-HSC composite structure depends on the bond between them, therefore, an extensive study has been performed to assess and improve the bond strength in two parts. In the first part, shear (push-out) and tensile (pull-off) bond strength tests have been conducted on ILC-HSC specimens which revealed that the interfacial bond strength is weaker than the weakest material i.e. ILC550. Hence, the bond strength has been improved by carbon and glass fiber-reinforced polymers (CFRPs and GFRPs) with two different grid dimensions i.e. 25 mm and 38 mm in the second part. Test results indicated that both the CFRPs and GFRPs significantly improved the bond strengths and this improvement depends on the reinforcement ratios. Maximum bond strength has been achieved for GFRP-25 reinforced ILCs where shear and tensile bond reinforcement ratios of 0.492% and 0.445% increased the shear and tensile bond strengths by 331% and 456% respectively as compared to un-strengthened specimens. In addition, the comparison of experimental shear bond strengths with five commonly used prediction models revealed the inaccuracy of all the presently available models. Moreover, there is no prediction model available for tensile bond strength prediction. Therefore, two new prediction models have been developed for shear and tensile bond strengths. The comparison of experimental results with developed models has revealed the accuracy and applicability of these models for both the un-strengthened and FRP strengthened ILC-HSC composite structures.

Keywords

Infra-lightweight concrete (ILC); High strength concrete (HSC); ILC-HSC composite; shear bond strength; tensile bond strength; FRP grid reinforced ILC-HSC; shear bond strength prediction model; tensile bond strength prediction model.

1 Introduction

The effectiveness of composite materials in terms of both the strength and durability depends on the bond between the materials as it is the weakest part [1–3]. Adequate bond performance is necessary to ensure satisfactory load transfer between different materials and resistance against delamination to improve serviceability [4]. Bond strength depends on friction/interlocking at the interface, adhesion between substrate and overlay, and reinforcement at the interface [5,6]. In the absence of reinforcement, adhesion between the substrate and the overlay is the most influencing factor which develops through penetration of cement of the overlay within the voids of the substrate (mechanical adhesion) and chemical bonding (specific adhesion) [7]. The reaction between the freshly prepared concrete of overlay and the un-hydrated cement particles of the substrate creates voids at the transition zone, making it the weakest part in the composite. Different parameters that influence these factors and consequently the quality of bonds include mechanical properties of concretes [8,9], interfacial roughness [10], surface pre-treatment [11,12], and environmental conditions [13].

To obtain superior bond performance, several studies have already been conducted on the application of novel materials as overlay i.e. geo-polymers [14], alkali-activated binders [15], and ultra-high performance concretes (UHPC) [16]. From amongst these materials, UHPC has proven to be a suitable option for overlay owing to its excellent properties including high strength, good durability, and lower long-term creep and shrinkage [17]. Enhanced bond strength due to the use

of UHPC has been investigated and supported by several researchers including strength between normal and UHPC by Zhang et al. [16], factors influencing bond strength between normal concrete (NC) and UHPC [18], and evaluation of this bond strength at elevated temperatures [19]. In addition to the application of novel materials, assessment of accurate bond strength also depends on the test method selected because the failure modes, as well as bond strength values, change with different test methods [20]. Many test methods are available in different codes to assess the bond strength under a range of stresses including tensile, shear, and combined shear and compression. Recently, Zanotti and Randl [20] drew a comparison between different test methods and recommended pull-off tests for tensile bond tests owing to their wide and easy applicability and push-out tests for shear as they are more representative of frictionless shear behavior.

The wide variety of material applications, the dependence of bond strength on mechanical properties of a range of materials and a huge scatter of test data necessitates the examination of bond strength for each variation of these parameters. Also, accurate evaluation of bond strength is necessary for the safer and durable design of composite structures and repair schemes. Although, several bond strength prediction models are available, however, they have been developed for specific material properties and combinations and there are limited studies that have developed bond strength prediction models for a range of materials [21]. In the present research program, shear and tensile bond tests have been conducted on specially manufactured infra-lightweight concrete (ILC) and high-strength concrete (HSC). To achieve efficient thermal performance and optimal strength to weight ratio of walls, ILC has been manufactured at Technische Universität Berlin (TU Berlin) [22]. ILC, manufactured using expanded clay lightweight aggregates (ECLAs) and lightweight sand, has extremely low density ($\leq 800 \text{ kg/m}^3$) and low thermal conductivity ($\leq 0.193 \text{ W/mK}$). As the density of manufactured concrete is lower than the density of lightweight

concrete ($>800 \text{ kg/m}^3$) as per BS EN 206 [23], therefore, this low-density concrete has been named as infra-lightweight concrete (ILC). Due to the low dead weight and high thermal efficiency, ILC has proven to be an efficient alternative of normal concrete (NC) and masonry for the construction of walls. The efficiency and practicality of ILC have already been demonstrated through research studies on its superiority over NC [24], development of its design and construction specifications [25], and its utilization in single-story houses built in Germany [26]. However, investigations on manufactured ILCs revealed practical problems concerning its durability and performance. The use of relatively higher w/c ratios and air content in ILC as compared to NC results in its inadequate long-term performance in terms of rough surface, surface cracks, and shrinkage. Also, the use of ECLAs and lower cement content in ILCs reduces its elastic modulus by 10 times as compared to NC, resulting in a softer material with a porous surface. Due to this lower strength and elastic modulus, ILC is affected by even low-velocity impacts which can further deteriorate its surface and strength. Experimental studies on shrinkage of ILCs, control of this shrinkage through FRP reinforcements, and development of shrinkage models for normal and reinforced ILCs have already been done by authors [27]. To further improve the properties of ILCs, a sandwich wall has been made in this study where ILC core has been encased with the HSC on both sides. As the use of ILC is crucial to achieve thermally insulated lightweight construction material, therefore, HSC has been selected as only a thin layer of HSC is sufficient to improve the properties of ILC while maintaining the lightweight and thermal efficiency of the constructed wall. Even with a thin layer of HSC, its potential benefits including high compressive strength, strong deformation resistance, low porosity, dense surface, good compaction performance, im-permeability, and good frost resistance can be utilized in the sandwich ILC-HSC wall.

The evaluation of the shear and tensile bond strengths of ILC-HSC specimens is highly required as the performance of newly manufactured ILC-HSC composite structures largely depends on the bond between them. In the first part of this research study, experiments have been conducted to evaluate the shear and tensile bond strengths of ILC-HSC specimens. These experimental studies have revealed that the interface between ILC and HSC is the weakest part as both the shear and tensile bond strengths are weaker than the weakest material in the composite specimens i.e. ILC. In the second part of this research study, the bond strength of the ILC-HSC composite structure has been improved. Since fiber-reinforced polymers (FRPs) are well known for shear [28] and tensile [29] strength enhancement of concrete structures, therefore, the ILC-HSC bond has been strengthened with carbon and glass fiber reinforcements using two different grid sizes i.e. 25 mm and 38 mm grids. Also, FRPs have been preferred over traditional steel reinforcements to maintain the light weight of the structure as well as its thermal properties as steel is heavier than FRPs, and the inclusion of steel creates a thermal bridge. Moreover, FRPs have high corrosion resistance [30], very high tensile strength [31], higher strength to weight ratio [32], and better flexibility [33], etc. The results of this study have shown that FRPs can significantly improve both the shear and tensile bond strengths and this improvement depends on the FRP reinforcement ratio at the ILC-HSC interface. Also, comparisons of the experimental shear bond strength of both the un-strengthened and strengthened ILC-HSC specimens with those obtained through five commonly used prediction models revealed that none of the models can predict the shear bond strength accurately. These five commonly used prediction models are Eurocode-2 (EN) model [34], ACI model [35], AASHTO model [36], Canadian Standards Association (CSA) model [37] and Australian Standards (AS) model [38]. For the tensile bond strength, there are no codified models. Therefore, in the third part of this research study, two new prediction models have been developed

to evaluate the shear and tensile bond strengths of both the un-strengthened and FRP grid reinforced ILC-HSC structures. Comparisons of developed prediction models with experimental results have shown that the developed models can be adopted for accurate prediction of un-strengthened and FRP grid reinforced ILC-HSC specimens.

2 Experimental tests

2.1 Materials

Two types of concretes have been manufactured for this experimental program namely ILC and HSC. The dry densities of ILC and HSC are 550 and 2335 g/cm³ and compressive strengths are 4.39 and 103.32 MPa respectively. Since the dry density of ILC is significant for its practical use, therefore, it has been named as ILC550 based on its dry density whereas HSC has been named as HSC C100 as per standard designation of compressive strength. Other mechanical (tensile strength, shear strength, and elastic modulus) and thermal (thermal conductivity coefficient) properties of both the ILC and HSC are given in Table 1. Dry densities of both the ILC and HSC specimens have been measured as per BS EN 12390-7 [39] in the temperature range of 105±5°C. For the compressive strength (f_c), cylinder compressive strengths of 150×300 mm cylinders have been measured at the age of 28 days as per BS EN 206 [40]. For the tensile strength, initially flexural tensile tests (i.e. the three-point bending tests) were conducted on 40×40×160 mm prisms as per BS EN 12390-5 [41]. The flexural tensile strength is then converted to axial tensile strength according to the BS EN 1992-1-1: 2004 [34]. Shear strength has been measured according to the method adopted by Mörsch [42]. Elastic moduli of 150×300 mm cylinders have been measured as per BS EN 12390-13 [43] at the age of 28 days. The thermal conductivity coefficient has been measured as per BS EN 12667: 2001 [44].

Table 1. Mechanical and thermal properties of ILC550 and HSC C100

	ILC 550	HSC C100
Dry density [g/cm ³]	550	2335
Compressive strength [MPa]	4.39	103.32
Tensile strength [MPa]	0.38	6.20
Shear strength [MPa]	0.52	12.40
Elastic modulus [MPa]	1900	42000
Thermal conductivity coefficient [W/(mK)]	0.128	1.62

ILC550 has been manufactured using expanded clay lightweight aggregates (ECLAs) and lightweight sand. Two types of ECLAs with varying particle sizes i.e. 1/4 (grain size between 1-4 mm) and 2/6 (grain size between 2-6 mm) have been used. Similarly, lightweight sand of particle size between 0-1 mm has been used as fine aggregates. The physical and chemical properties of both the ECLAs and lightweight sand are the same as used by authors in their previous study [27]. Although lightweight concrete is manufactured using high air entrainment generally, however, use of ECLAs in ILC decreases the requirement for air-entrainment. Blast furnace slag cement of type CEM III/A and 32.5 N grade has been used [45]. CEM III is a mix of blast furnace slag and OPC and A refers to the type of cement (CEM III) with at least 40% slag and grade 32.5 N indicates the early age strength of 32.5 N. Plasticizer and Stabilizer have been used as admixtures to improve the workability and reduce the segregation, respectively. The mix design composition of ILC550 is given in Table 2.

HSC can be defined as concrete with extremely high 28-days compressive strength, improved modulus of elasticity, higher impact resistance, and lower shrinkage as compared to NC. This

extremely high value of concrete strength can be achieved by altering the properties and mix proportions of the ingredients used in NC. The strength and size of aggregates, cement-aggregate bond, lower w/c ratio, and use of admixtures for strength enhancement are the main parameters that influence the strength of concrete. The mix design of HSC used is given in Table 2. For the HSC under-study, a very low w/c ratio of 22% has been used. A special type of cement known as flowstone cement made by a mixture of Portland cement and ultrafine binder has been used. This type of cement enhanced binding properties and plays a critical role in improving the strength of concrete. To maintain the workability of concrete for a given w/c ratio, plasticizer has been used and the amount of plasticizer used for HSC is significantly higher than the ILC as the w/c ratios are at two different extremes. To remove undesired air voids from concrete to achieve high strength, defoamer has also been added to concrete. American concrete institute (ACI 363R-10) [46] defines HSC as concrete with compressive strength of 55 MPa (8000 psi) or higher. Similarly, BS EN 1992-1-2 [47] classifies HSC into three classes starting from concrete strength 55 MPa (C55/67). Therefore, manufactured concrete with compressive strength of 103.32 MPa can be defined as HSC as per both the standards.




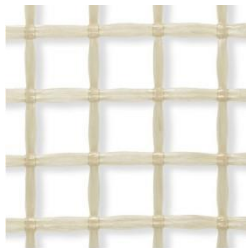
Table 2. Mix designs of ILC550 and HSC C100

	ILC550			HSC C100	
	V (L)	M (kg)		V (L)	M (kg)
Light sand	6.3	6.7	Quartz sand	449	1165
ECLA 1/4	144.7	123.0			
ECLA 2/6	389.4	210.3	Flowstone grey cement	300	1050
CEM III-A 32.5N	50.6	154.3			
Water	204.0	204.0	Water	230	230

Silica fume	32.0	75.2	Plasticizer	17	17.5
Plasticizer	2.5	2.7			
Stabilizer	0.21	0.19	Defoamer	4	3.5
Air	240	0			
Sum	1000	776	Sum	1000	2466

To improve the bond between ILC and HSC, two types of fiber-reinforced polymers i.e. carbon and glass fiber reinforced polymers (CFRPs and GFRPs) have been used. Two different grid arrangements have been used for each type of FRP with varying arrangements of FRP bars. These two different grid arrangements are presented in Table 3. As the distance between all the longitudinal and transverse strands are 25 mm in arrangement 1 and 38 mm in arrangement 2 of each type of FRP, therefore, they have been named as FRP-25 (CFRP-25 and GFRP-25) and FRP-38 (CFRP-38 and GFRP-38), respectively. Grid dimensions, cross-sectional areas of the strands, strand widths and thicknesses, strengths and elastic moduli of all the four FRP grids are presented in Table 4. From this table, it can be seen that although the cross-sectional areas of both the CFRPs and GFRPs for each type of grid arrangement are very close, the strength, as well as elastic modulus of CFRP, is twice than that of GFRP.

Table 3. FRP grid arrangements

Grid type	CFRP-25	CFRP-38	GFRP-25	GFRP-38
Plane grid				

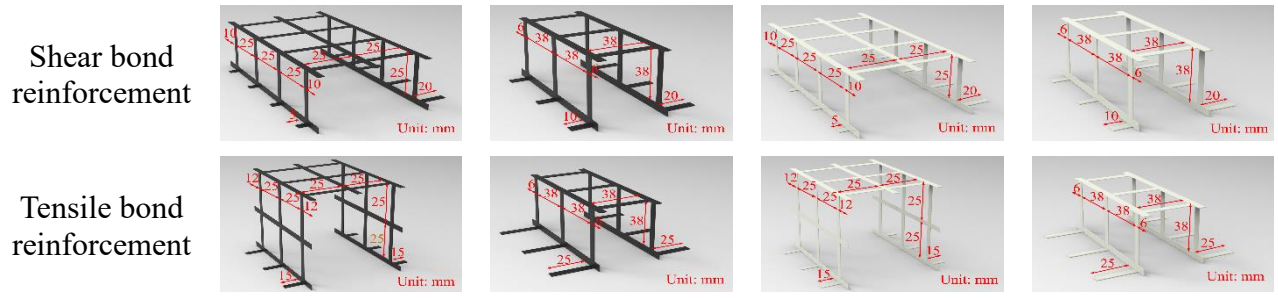


Table 4. Dimension and mechanical properties of FRP grids

FRP grid type	Width of one grid (mm)	Cross-sectional area of strand (mm ²)	Strand width (mm)	Strand thickness (mm)	Strength (MPa)	Elastic modulus (GPa)
CFRP-25	25	3.62	6.03	0.6	2300	120
CFRP-38	38	3.62	6.03	0.6	2300	120
GFRP-25	25	3.69	6.15	0.6	1100	60
GFRP-38	38	3.69	6.15	0.6	1100	60

2.2 Sample preparation and testing procedures

The bond strength between two materials can be determined under a range of stresses including shear, tensile, compressive, and combined compressive and shear stresses. Currently, shear and tensile bond strength tests are widely adopted to evaluate the bond strength between composite materials [2]. Therefore, shear and tensile bond tests have been conducted to test the bond between ILC and HSC under study. For the shear bond strength test, a range of test methods is available including single shear, double shear, bond-slip, and core drilling tests. From amongst these tests, the double-shear (push-out) test method has been selected as its specimen is easy to cast with less interference [21], the test is easy to perform and is widely adopted to evaluate shear strength between composite materials [48]. For the tensile bond strength test, direct tensile strength has

been measured using the pull-off test method from amongst a variety of tensile bond strength tests e.g. pure, direct, and indirect tensile strength tests, etc.

To ensure the accuracy and reduce the discreteness amongst the test samples, single batches of ILC and HSC have been prepared for both the shear and tensile bond tests and the samples for the test have been taken from the respective batch. The ingredients of both the ILC and HSC have been mixed carefully according to the respective ratios, and each ingredient has been weighed using weigh balance. Furthermore, if the mechanical properties and dry density of the batches varied by more than 5% from the standard properties of ILC and HSC, the batch was discarded. The workability of both the ILC and HSC was good, and they can be called as self-compacting concretes (SCCs). The added super-plasticizer has made both the concretes to flow easily in and around the formwork, eliminating the requirement of vibration or tamping after pouring. The slump flow test was conducted, and a slump values of 600-700 mm and 650-750 were obtained for ILC and HSC, respectively.

2.2.1 Push-out shear bond tests

The push-out shear tests have been conducted as per BS EN 12090 [49], along-with the determination of specimen sizes. The schematic plan and preparation of the test samples for push-out tests are presented in Figure 1 and Figure 2 respectively. An HSC C100 block of 80 mm height has been made composite with two ILC550 blocks on each side making a bonding height of 60 mm (Figure 1). The preparation of experimental specimens for push-out tests is presented in Figure 2. Initially, two ILC blocks on each side of HSC were cast and cured for two days under 20°C temperature and 65% humidity. As the ILC blocks gained basic strength after two days, the HSC block was cast between them resulting in a natural bond without any adhesive. For bond strength behavior, the classification of concrete surfaces at the interface is critical to define surface

roughness. BS EN 1991-1-1 [34] and fib model code 2010 [50] classifies concrete surfaces as very smooth, smooth, rough, and very rough. The specimen prepared for the shear bond test has been classified as smooth as no surface treatment has been done (Figure 2(a)). The untreated surfaces result in the economical production of the specimen and also provide uniformity among the tests as the surface of FRP strengthened specimens can hardly be treated. The untreated surfaces can be classified as smooth according to both BS EN 1991-1-1 [34] and fib model code 2010 [50]. The experimental specimen is presented in Figure 2(b) on which load was applied on the HSC top surface until failure (Figure 2c).

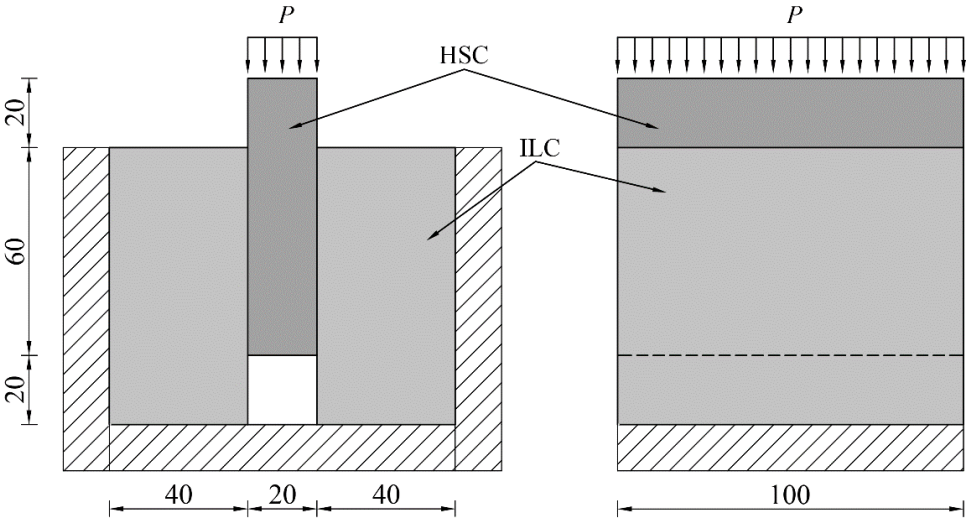


Figure 1 Schematic plan of ILC-HSC push-out test specimen (unit: mm)

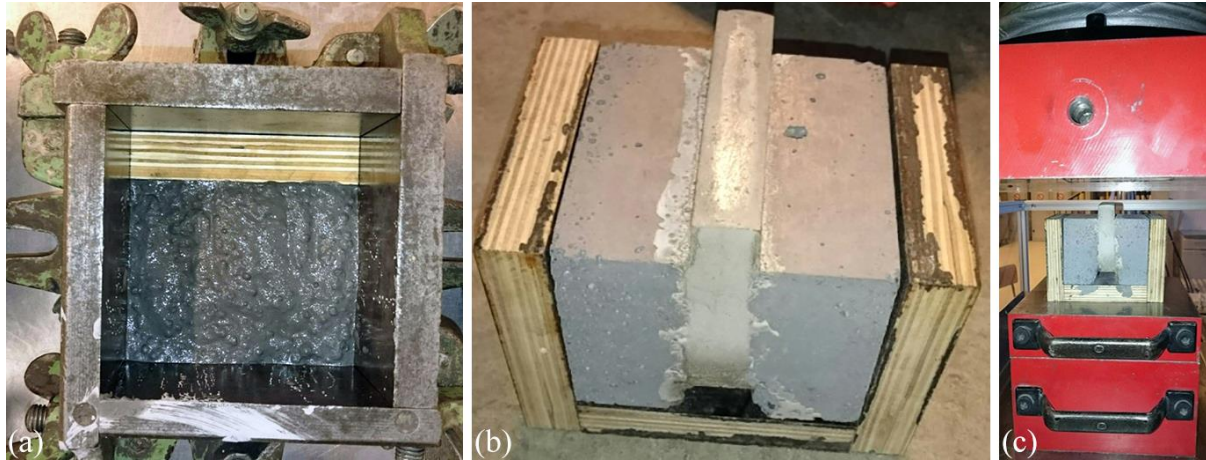


Figure 2 Shear bond strength test (a) casting with a rough surface (b) specimen (c) testing

2.2.2 Pull-off tensile bond tests

Pull-off tensile strength tests have been conducted as per BS EN 1015-12 [51] as it gives the direct tensile strength of the material itself or the strength of the interface between materials. The sample sizes have also been selected according to BS EN 1015-12 [51] and the schematic plan of the pull-off test and test sample preparation are presented in Figure 3 and Figure 4, respectively. For this pull-off test, HSC overlay with a thickness of 20 mm was cast over the ILC substrate of 40 mm height (Figure 3) making a rectangular block of dimensions $100 \times 100 \times 60$ mm. Similar to push-out tests, the surface of the specimens have been kept untreated and classified as smooth (Figure 4a). After casting, a shallow core was drilled perpendicularly into through the full depth of HSC C100 and 2 mm into the ILC550 (Figure 3 & Figure 4b). After drilling the core, a metal disc of the same diameter as the drilled core (50 mm) was attached to the surface of HSC C100. Once the metal disc was bonded, the tensile load was applied to the disc at the rate of 0.02 MPa per second until failure (Figure 4c).

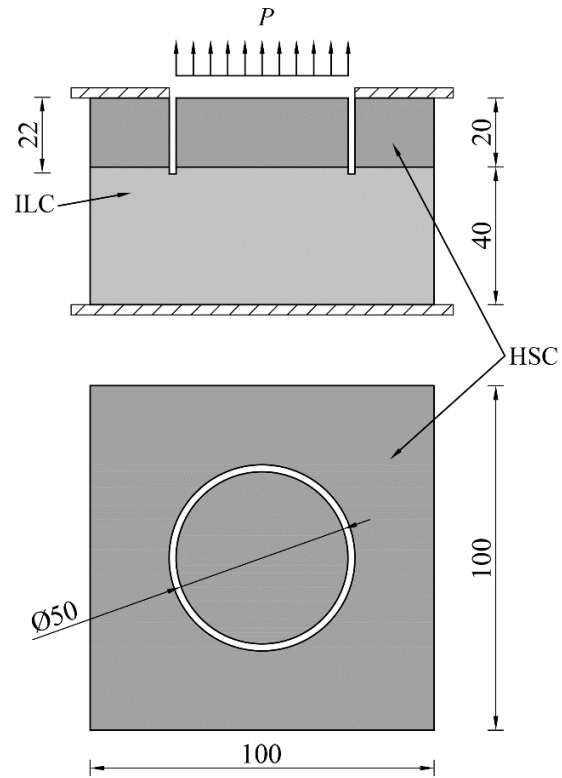


Figure 3 Schematics of pull-off tension test (unit: mm)

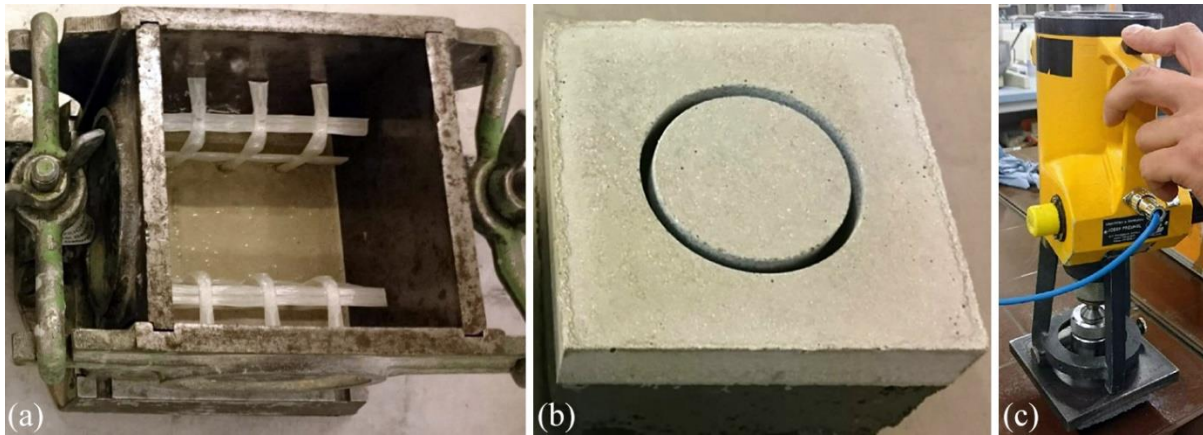


Figure 4 Tensile bond strength test (a) casting with rough surface (b) specimen (c) testing

2.2.3 Strengthening schemes

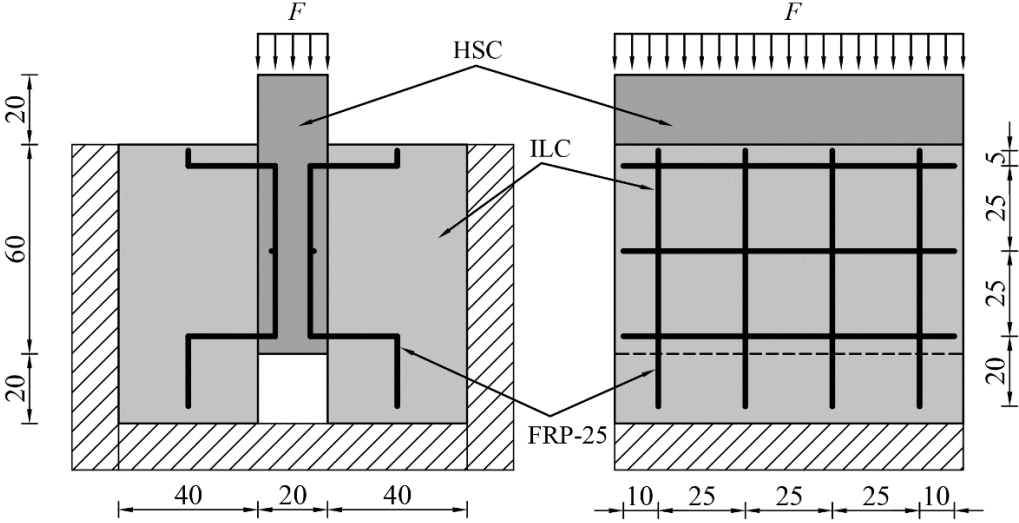
Both the tensile and shear bond samples were then reinforced with CFRP and GFRP strands to improve bond strength. The strengthening scheme has been designed to maintain a balance between strength improvement of the sandwich wall and constructability. As the FRP reinforcement is the most influencing factor in improving the strength of the ILC-HSC wall, therefore, FRP reinforcement has been designed to shift the failure planes from the interface to either ILC or the HSC. For the shear bond strength, the failure mechanism can be shifted from the interface failure to either the cohesive failure of the ILC or the HSC. Since the compressive strength of ILC is considerably less than that of HSC (Table 1) and the FRPs cannot contribute to the compressive strength, therefore, the shear failure mechanism of the FRP reinforced ILC-HSC specimen can be based on the compressive strength of ILC. However, for the tensile strength, the tensile FRP reinforcement contributed to the tensile strength of ILC and has been designed so that the failure plane shifts to HSC.

2.2.3.1 Experimental Strengthening scheme:

Dimensions and mechanical properties of both these strands with two different grid arrangements are presented in Table 3 and Table 4. As the geometry of both the CFRP and GFRP reinforcements for each type of grid reinforcement is similar, therefore, similar strengthening schemes have been adopted and named FRP-25 and FRP-38. For all the FRP reinforced specimens, a hard FRP grid has been used. Initially, soft FRP grids were bent in the mold in the desired shapes where they were allowed to cure. This curing process of extremely thin FRP grids resulted in negligible stress concentrations at the FRP grid corners. Shear strengthening schemes with FRP-25 and FRP-38 grid reinforcements are presented in Figure 5a and Figure 5b respectively. As there are two ILC550 blocks around one HSC C100 block, two FRP grid reinforcements have been used. The center of

two transverse strands in FRP-25 grids coincides with the center of the sample which results in a total of four transverse FRP-25 strands in each ILC550 block. For FRP-38 reinforcement, three transverse strands have been used in each ILC550 sample with the central strands coinciding with the center of the ILC550 block. The number of strands in each block affects the shear reinforcement area at the interface and consequently the shear bond strength.

Tensile strengthening schemes using FRP-25 and FRP-38 grids are presented in Figure 6a and Figure 6b respectively. For both types of grid reinforcements, at least two longitudinal strands of FRPs pass through the central core. As the diameter of the core is a multiple of transverse spacing of the FRP-25 grid, special attention has been paid towards arrangements of FRP grids. FRP-25 grids have been arranged so that the center of two transverse strands coincides with the center of the core (Figure 6a). For FRP-38, a single central transverse strand is exactly in the center of the ring (Figure 6b). This grid arrangement also affects the area of reinforcement within the tensile load area.



(a)

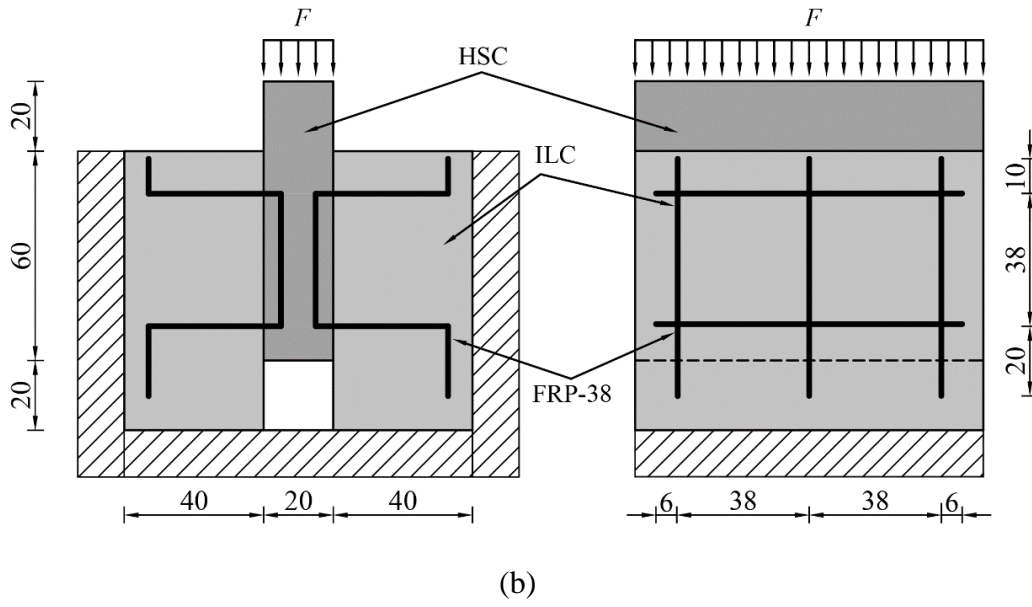
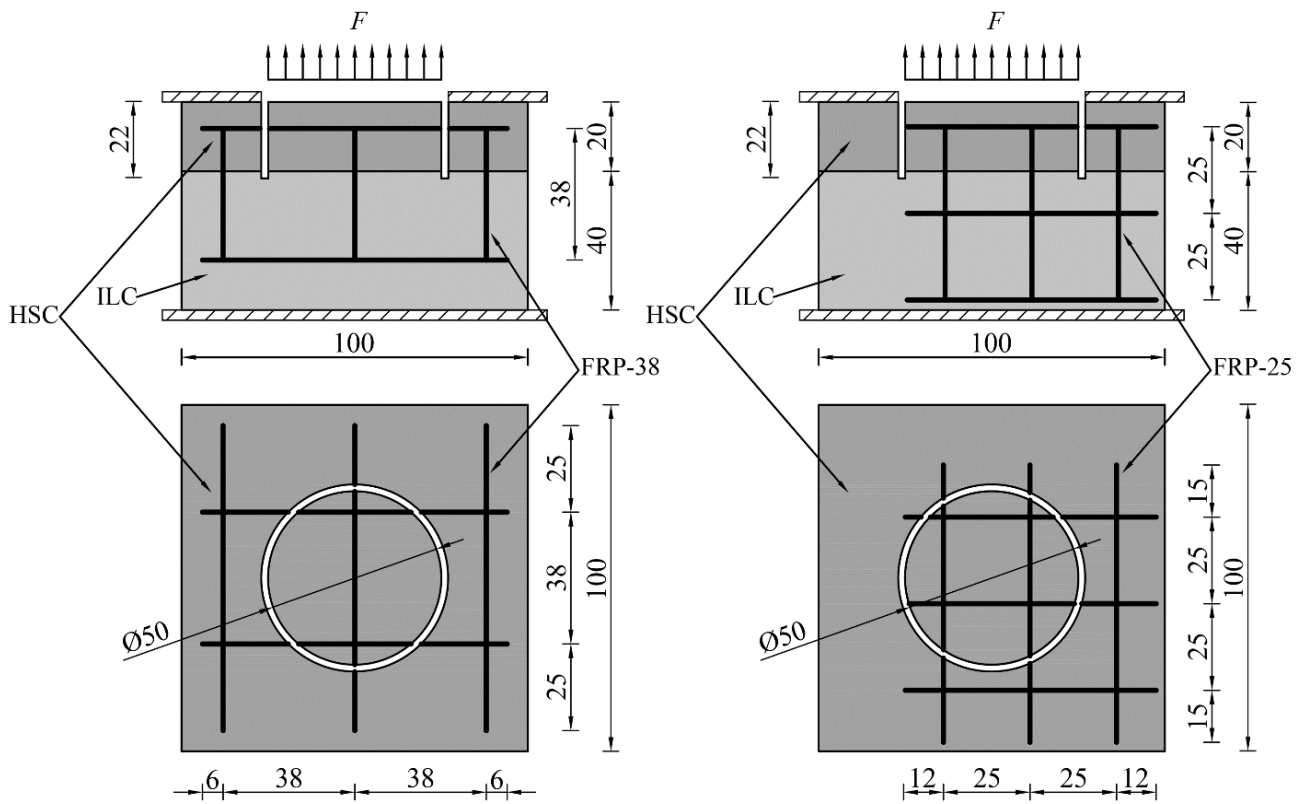


Figure 5 Shear strengthening of ILC-HSC bond (a) FRP-25 (b) FRP-38



(a)

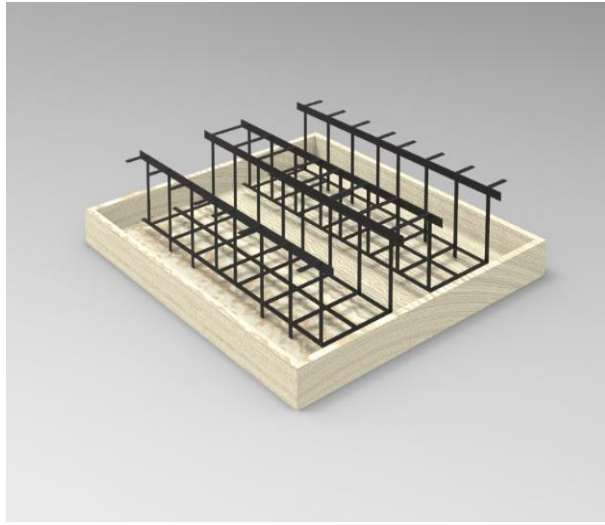
(b)

Figure 6 Tensile bond strengthening scheme (a) FRP-25 (b) FRP-38

Both the shear and tensile bond strength tests have been conducted on three samples each of un-strengthened ILC-HSC specimens (2 tests \times 3 samples each), CFRP reinforced ILC-HSC specimens with two different grid arrangements (2 tests \times 3 samples each \times 2 grid arrangements) and GFRP reinforced ILC-HSC specimens with two different grid arrangements (2 tests \times 3 samples each \times 2 grid arrangements). This makes a total of 15 samples for the shear bond test and 15 samples for the tensile bond test. For test results, the average of each type of test specimen has been taken.

2.2.3.2 Practical Strengthening scheme:

The construction of the FRP reinforced ILC-HSC wall is similar to the construction of the sandwich wall of normal concrete. First of all, FRP grid reinforcement is arranged in two separate and similar casting molds of the HSC panels (Figure 7a) followed by the pouring and curing of the HSCs (Figure 7b). Secondly, the two HSC panels are erected and FRP grid reinforcements are connected using ties with the spacing according to the thickness of the ILC (Figure 7c). Then, the mold for ILC is positioned and fixed followed by the curing of ILC (Figure 7d). Once the ILC is cured, the ILC-HSC sandwich wall with FRP grid reinforcements is obtained (Figure 7e). Furthermore, the good workability of both the ILC and HSC makes them self-compacting concrete (SCC). Therefore, both the concretes can flow easily in and around the formwork eliminating the need for vibration and tamping after the pouring.



(a)



(b)



(c)



(d)



(e)

Figure 7 Construction sequence of FRP reinforced ILC-HSC wall (a) Fixing FRP in HSC molds (b) pouring of HSC (c) erection of HSC walls (d) pouring of ILC (e) FRP reinforced ILC-HSC wall

3 Experimental results and discussion

Experimental tests have been conducted to assess bond strength between ILC having a dry density of 550 g/cm^3 (ILC550) and HSC with compressive strength of 103.32 MPa (HSC C100). Bond

strengths have been assessed under two types of stresses i.e. shear and tensile stresses. Shear bond strengths have been conducted using push-out tests recommended by BS EN 12090 [49] and tensile bond strengths have been assessed using pull-off tensile strength tests as per BS EN 1015-12 [51].

3.1 ILC-HSC shear bond test results

For shear bond failure, the specimen can fail in one of the two possible failure mechanisms i.e. adhesive failure at the interface or cohesive failure in one of the composite materials. The type of failure mechanism depends on bond strength as well as the strength of individual materials in the composite specimen. The shear strength of the ILC550 specimen is 0.52 MPa and that of the HSC C100 specimen is 12.40 MPa (Table 1). Experimental failure mechanism in push-out strength tests of un-strengthened specimens indicated that bond shear strength is weaker than the weakest material in the specimen i.e. ILC550 as the shear failure plane passed through the ILC-HSC interface (Figure 8a). On the other hand, the failure mechanism changed to cohesive failure when specimens were reinforced with FRPs. In each of the FRP reinforced samples, it was observed that failure of the specimen is through the compression failure of ILC550 material (Figure 8b-e), as the load applied at the top of HSC induces compressive stresses in ILC. This exhibits the effectiveness of FRPs in increasing the shear bond strength of ILC-HSC. The inclusion of FRPs converts the failure from interface shear failure to compressive failure of ILCs, which is significantly greater than the shear bond strength. Furthermore, the shear strength of un-strengthened and strengthened ILC-HSC specimens can be quantified easily by dividing the ultimate shear load obtained in the experiment by bonded shear area (Eq. 1).

$$\tau_b = \frac{P_u}{2bh} \quad (1)$$

where τ_b is the shear bond strength, P_u is the shear failure load, b is the width of the bonded surface i.e. 100 mm and h is the height of the bonded surface i.e. 60 mm. Shear bond strengths of un-strengthened and strengthened ILC-HSC specimens are presented in Table 5, where P indicates the ultimate load in the push-out test and τ_b is the shear strength calculated using Eq. 1.

The test results include the strength of 3 specimens for each test type, average of the 3 samples, standard deviations (SDs), coefficients of variations (CVs), and improvement of ILC-HSC shear bond strength due to FRPs. The low values of CVs indicate that the errors among the experiments are significantly low. The reason for low errors is the measures that have been taken to ensure consistency among test samples. From these calculated shear strengths (Table 5), it can be concluded that FRPs can significantly improve the shear bond strength of the ILC-HSC bond. The FRP reinforcement ratios (ratio of reinforcements crossing the interface) of 0.483%, 0.362%, 0.492%, and 0.369% for CFRP-25, CFRP-38, GFRP-25 and GFRP-38 respectively have increased the shear bond strengths by 318%, 182%, 331% and 184% respectively. Although the strength of CFRPs is twice than that of GFRPs, results indicate that shear bond strength gain is similar for CFRP-25 and GFRP-25 as well as for CFRP-38 and GFRP-38. Thus, it can be concluded that an increase in shear bond strength between the composite specimens depends on the FRP shear reinforcement ratio irrespective of FRP type.

This shear bond strength improvement is also considerably higher than the shear strength of ILC550 ($\tau_{c, ILC}$) (Figure 9). The shear bond strength of un-strengthened ILC-HSC specimen (τ_b) is 94% of the shear strength of ILC ($\tau_{c, ILC}$) and this bond strength has increased by 318%, 182%, 331%, 184% for CFRP-25, CFRP-38, GFRP-25, and GFRP-38 respectively.

Since the push-out tests have been conducted and interpreted according to BS EN 12090 [49], therefore, the stress concentrations at the edges have been ignored. These stress concentrations at

the edges are so low that their inclusion does not make any difference in the bond test results, and they have also been ignored by previous researchers [20,21].

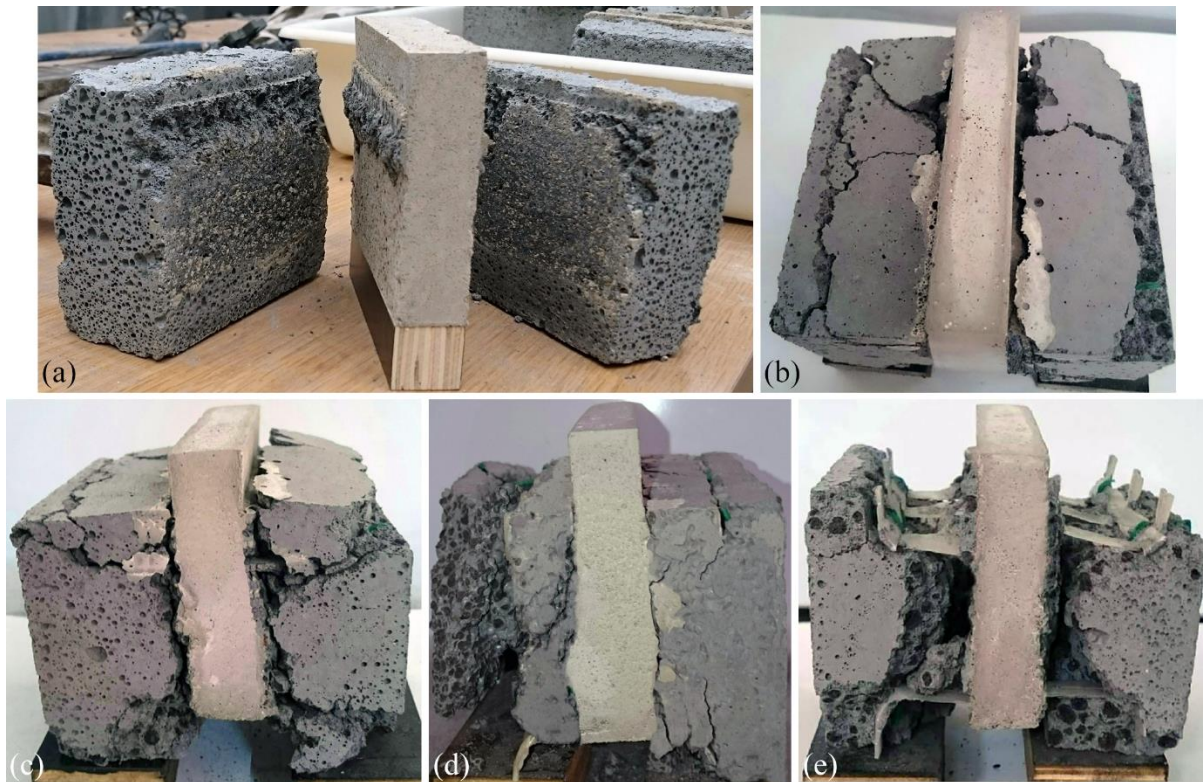


Figure 8 Specimen failure in Shear bond tests (a) ILC-HSC (b) ILC-HSC with CFRP-25 (c) ILC-HSC with CFRP-38 (d) ILC-HSC with GFRP-25 (e) ILC-HSC with GFRP-38

Table 5 Shear bond strengths of ILC-HSC specimens

		ILC-HSC	ILC-HSC with CFRP-25	ILC-HSC with CFRP-38	ILC-HSC with GFRP-25	ILC-HSC with GFRP-38
P_u (N)	Specimen 1	6234	25206	17426	27070	15789
	Specimen 2	5641	23835	16438	24005	17672

Specimen 3	5758	24769	15835	24891	16583
Average	5878	24603	16566	25322	16681
SD	256	572	656	1288	772
Specimen 1	0.52	2.10	1.45	2.26	1.32
Specimen 2	0.47	1.99	1.37	2.07	1.47
Specimen 3	0.48	2.06	1.32	2.00	1.38
Average	0.49	2.05	1.38	2.11	1.39
SD	0.02	0.05	0.05	0.11	0.06
CV	0.044	0.023	0.040	0.051	0.046
Improvement	-	318%	182%	331%	184%

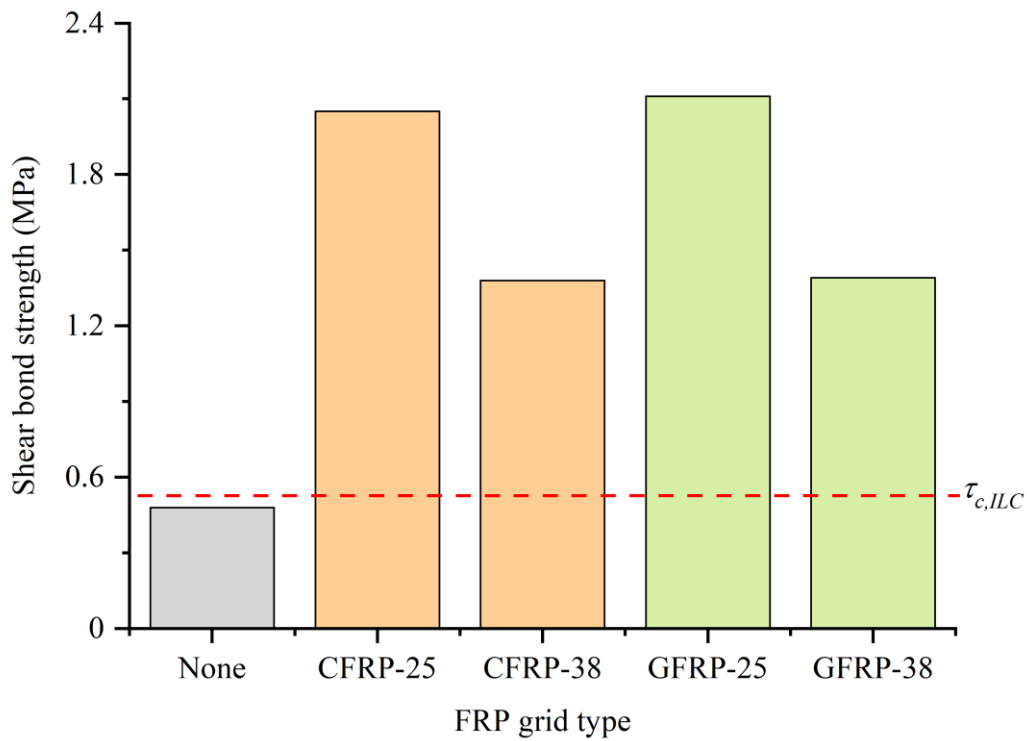


Figure 9 ILC-HSC shear bond strength comparison

3.2 ILC-HSC tensile bond test results

For tensile bond strength, failure can be either by adhesion failure between substrate and overlay, tensile splitting failure of either the substrate or the overlay, or the combination of these. In the un-strengthened sample, the failure plane passes through the ILC-HSC interface in tensile loading (Figure 10a). Similar to shear bond strengthening, the shift of failure plane was observed where failure in all the strengthened specimens is a tensile failure in HSC C100 overlay (Figure 10b-e) just above the FRP reinforcement layer as the FRP reinforcement has been designed to shift the failure plane to HSC. Although the tensile strength of ILC550 (0.38 MPa) is lower than that of HSC C100 (6.20 MPa), the embedment of FRP reinforcement throughout the ILC550 depth has also increased its tensile strength. The tensile strength of all the specimens can be calculated by dividing the experimental ultimate tensile load by the core area (Eq. 2)

$$f_{bt} = \frac{F_u}{A} \quad (2)$$

Where f_{bt} is the bond tensile strength, F_u is the tensile failure load, A is the test area of cylindrical specimen i.e. 1963.50 mm². Average failure loads and tensile strengths of un-strengthened and strengthened specimens are given in Table 6. Similar to shear bond test results, low values of CVs for tensile bond test results indicate that the errors are minimal. The bond strength of the un-strengthened specimen (f_{bt}) is 0.16 MPa, which is around 42% of the tensile strength of ILC ($f_{ct,ILC}$) i.e. 0.38 MPa. This lower strength of the ILC-HSC tensile bond as compared to the tensile strength of the ILC is also evident in the failure mode of the un-strengthened specimen where the failure plane passes through the interface layer between ILC and HSC (Figure 10a).

Pull-off tests on FRP strengthened ILC-HSC samples indicate that this bond strength can be significantly increased. Similar to shear bond strength, this increase in tensile bond strength also

depends on the tensile bond reinforcement ratio of FRPs and does not vary considerably for FRP type. This tensile bond reinforcement ratio is the ratio of the plane area of reinforcement to the concrete in the tensile loading area, whereas the shear reinforcement ratio is the ratio of reinforcement crossing the interface to the shear loaded area. The tensile bond reinforcement ratios of CFRP-25, CFRP-38, GFRP-25 and GFRP-38 grids are 0.436, 0.320, 0.445, and 0.326 respectively and the corresponding tensile bond strengths are 0.86, 0.64, 0.89 and 0.67 MPa respectively. This indicates a strength increase of 438%, 300%, 456%, and 319% for CFRP-25, CFRP-38, GFRP-25, and GFRP-38 grids respectively with the maximum strength gain for GFRP-25. In the failure modes of strengthened specimens, this increase in bond strength is evident as the failure plane shifted from the ILC-HSC interface to tensile failure in HSC C100 (Figure 10 b-e).

Comparison of un-strengthened and strengthened tensile bond strengths with the tensile strength of ILC ($f_{ct, ILC}$) is presented in Figure 11. From this comparison, it is evident that FRP strengthening has also significantly improved the bond strength as compared to the tensile strength of ILC ($f_{ct, ILC}$). This increase in strength is 126%, 68%, 134% and 76% for CFRP-25, CFRP-38, GFRP-25 and GFRP-38 grids, respectively.

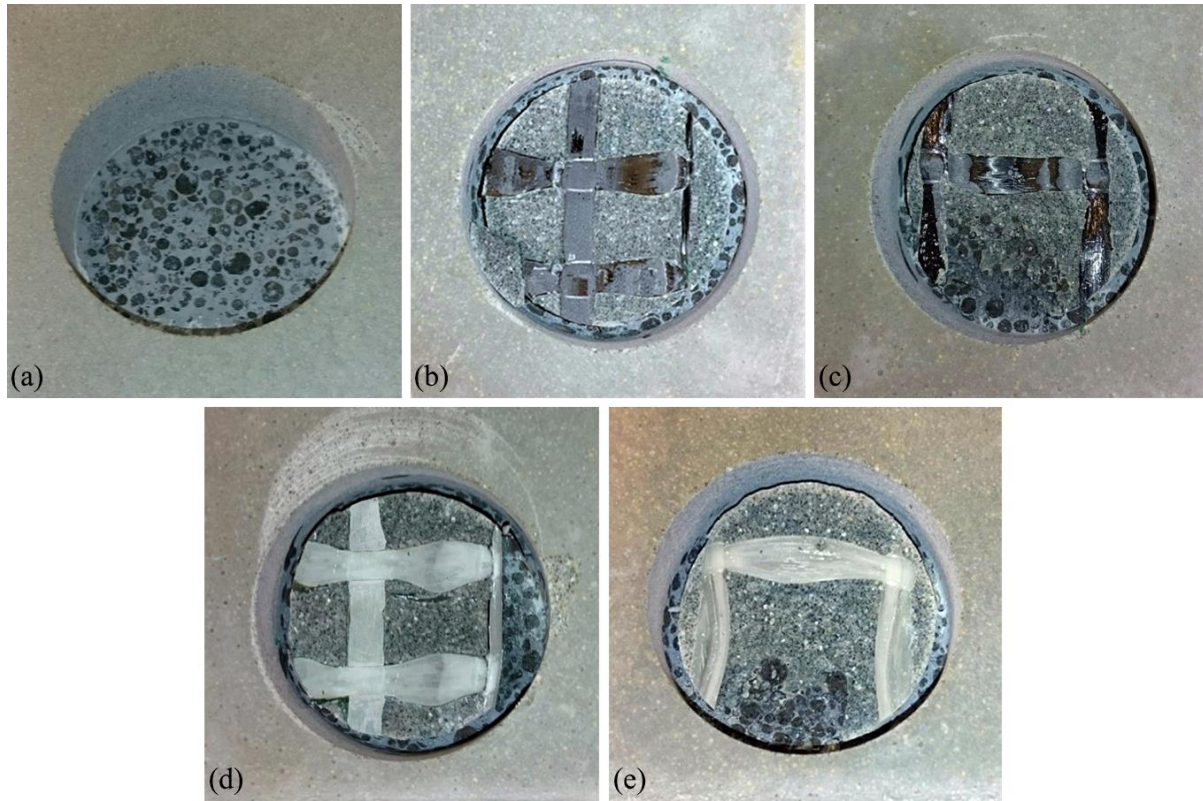


Figure 10 Specimen failure in tensile bond tests (a) ILC-HSC (b) ILC-HSC with CFRP-25 (c) ILC-HSC with CFRP-38 (d) ILC-HSC with GFRP-25 (e) ILC-HSC with GFRP-38

Table 6 Tensile bond strengths of ILC-HSC specimens

	ILC-HSC	ILC-HSC with CFRP-25	ILC-HSC with CFRP-38	ILC-HSC with GFRP-25	ILC-HSC with GFRP-38
Specimen 1	285	1689	1335	1826	1178
Specimen 2	339	1767	1257	1767	1355
F_u (N) Specimen 3	318	1610	1178	1649	1414
Average	314	1689	1257	1748	1316
SD	22	64	64	73	100
Specimen 1	0.15	0.86	0.68	0.93	0.60

f_{bt} (MPa)	Specimen 2	0.17	0.90	0.64	0.90	0.69
	Specimen 3	0.16	0.82	0.60	0.84	0.72
	Average	0.16	0.86	0.64	0.89	0.67
	SD	0.01	0.03	0.03	0.04	0.05
	CV	0.071	0.038	0.051	0.042	0.076
Improvement	-	438%	300%	456%	319%	

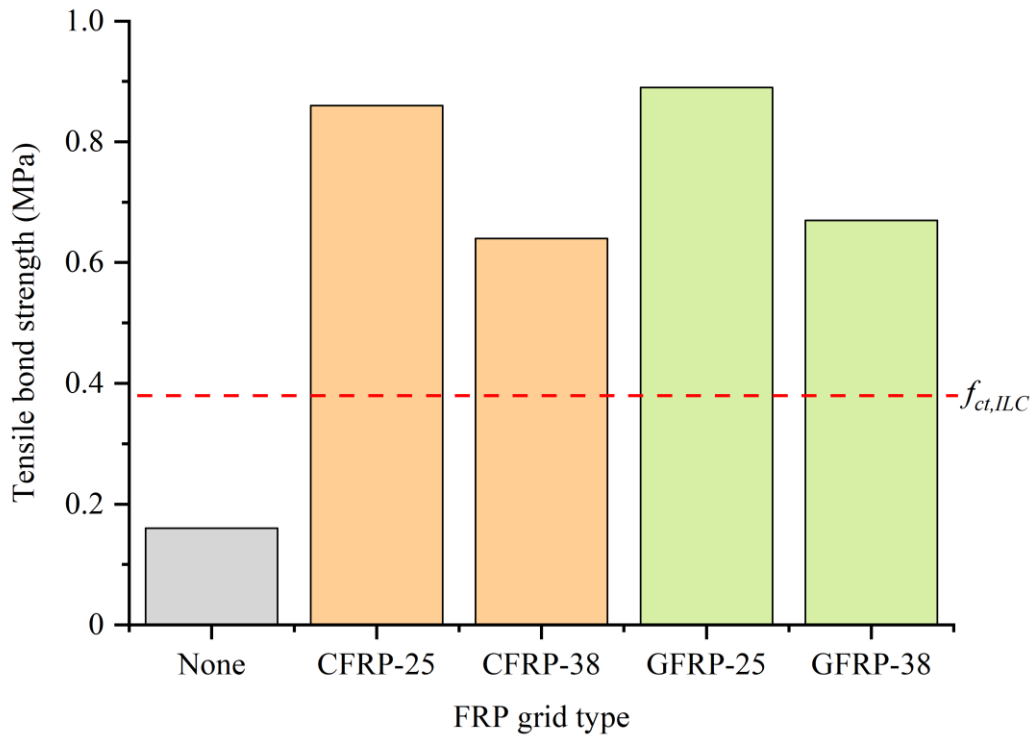


Figure 11 ILC-HSC tensile bond strength comparison

4 Development of bond strength prediction models

The strength and serviceability of structural components made with composite materials mainly depend on the bond between them as the bonding surface is usually the weaker portion of the composite specimen. Accurate prediction of the bond strength is vital to ensure the safer and durable performance of the structure.

4.1 Shear bond strength prediction models

There are several models to evaluate the shear bond strength of the interface between two materials and the most commonly used models are the Eurocode-2 (EN) model [34], ACI model [35], AASHTO LRFD model [36], Canadian standards association (CSA) model [37] and the Australian standard (AS) model [38]. Prediction of strength in all these models depends on several factors including mechanical properties of concrete and steel, concrete dimensions, reinforcement ratio, the angle between shear reinforcing bars and interface plane, and roughness of the interfaces. All of these parameters have been assessed in the experimental program to evaluate and compare shear bond strengths calculated using these five models with experimental results.

4.1.1 Existing shear bond strength prediction models

4.1.1.1 EN model

Shear bond strength prediction between two concretes without normal force in BS EN 1992-1-1 model [34] is based on the tensile strength of concrete and yield strength of shear reinforcement. However, the upper limit of this strength is specified based on the compressive strength of the concrete (f_c). This shear bond strength (τ_b) can be calculated by Eq. 3.

$$\tau_b = cf_{ct} + \rho f_y (\mu \sin \alpha + \cos \alpha) \leq 0.5vf_c \quad (3)$$

Where c and μ are factors which depend on the roughness of the interface between two concretes, f_{ct} is the smaller of tensile strengths of concretes, ρ is the shear reinforcement ratio at the interface, f_y is the yield strength of shear reinforcement, α is the angle between shear reinforcing bars and interface plane, v is shear strength reduction factor based on compressive strength of concrete, and f_c is the smaller of compressive strengths of concretes at the interface.

4.1.1.2 ACI model

As per the American concrete institute (ACI) model [35], the shear bond strength between two concretes depends on the compressive strength of concrete, yield strength of steel, and areas of shear reinforcement and concrete. The shear bond strength (τ_b) can be computed using Eq. 4.

$$\tau_b = 0.17\lambda\sqrt{f_c} + \frac{A_{vf}}{A_c} f_y (\mu \sin \alpha + \cos \alpha) \quad (4)$$

Where λ is a modification factor for lightweight concrete (1.0 for normal-weight concrete, 0.85 for sand-lightweight concrete, and 0.75 for all-lightweight concrete), f_c is the compressive strength of concrete, A_{vf} is the area of shear-friction reinforcement perpendicular to the shear plane, A_c is the area of concrete at shear transfer plane, f_y is the yield strength of shear reinforcement and α is the angle between the shear reinforcing bars and the interface plane.

4.1.1.3 AASHTO model

In the Bridge design specifications of the American Association of State Highway Transportation Officials (AASHTO) [36], the shear bond strength between the concretes depends on the cohesion and friction of concrete materials, areas of shear reinforcement and concrete and tensile strength of steel. The shear bond strength (τ_b) is calculated using Eq. 5.

$$\tau_b = c + \frac{A_{vf}}{A_{cv}} \mu f_y \leq \min(K_1 f_c, K_2) \quad (5)$$

Where c is a cohesion factor accounting for lightweight concrete, A_{vf} is the area of shear reinforcement crossing shear plane, A_{cv} is the area of concrete at the shear interface, μ is the friction factor, f_y is the yield strength of shear reinforcement, K_1 is a fraction of concrete strength available to resist interface shear, f_c is the compressive strength of the concrete and K_2 is a factor limiting interface shear resistance.

4.1.1.4 CSA model

According to the Canadian Standards Association (CSA) standard for the design of concrete structures [37], the shear bond strength (τ_b) of the concrete interface plane shall be computed from using Eq. 6.

$$\tau_b = \lambda(c + \mu \rho_v f_y \sin \alpha_f) + \rho_v f_y \cos \alpha_f \leq 0.25 f_c \quad (6)$$

Where λ is a factor for light-weight concrete, c is a factor for cohesion, μ is the coefficient of friction, ρ_v is the ratio of shear reinforcement, f_y is the yield strength of shear reinforcement, α_f is the angle between shear friction reinforcement and shear plane and f_c is the compressive strength of the concrete.

4.1.1.5 AS model

In the Australian Standard for concrete structures [38] model, the shear bond strength (τ_b) of the concrete interface plane can be calculated using Eq. 7.

$$\tau_b = k_{co} f_{ct} + \mu \frac{A_{sf} f_{sy}}{s b_f} \quad (7)$$

Where k_{co} is the cohesion coefficient, f_{ct} is the tensile strength of concrete, μ is the coefficient of friction, A_{sf} is the area of fully anchored shear reinforcement perpendicular to the interface, f_{sy} is the yield strength of shear reinforcement not exceeding 500 MPa, s is the spacing of anchored shear reinforcement perpendicular to interface and b_f is the width of the shear plane.

4.1.2 Results of existing shear bond strength prediction models

Shear bond strength in both the un-strengthened and fiber-reinforced ILC550 and HSC C100 specimens have been calculated using five commonly used prediction models. Results of these prediction models and their comparison with experimental results along with their mean absolute deviations (MAD) are presented in Table 7 and Figure 12. From this comparison, it is evident that not only existing prediction models fail to accurately predict ILC-HSC shear bond strength, but the calculated values differ considerably from the actual bond strength as indicated by MAD. This mean absolute deviation is highest for the AASHTO model [36] i.e. 0.688 and lowest for the EN model [34] i.e. 0.418.

This difference in predicted and calculated values is due to the use of different concrete strengths and fiber reinforcements. Although the calculation of shear bond strength using various prediction models depends on several factors including mechanical properties of concrete and steel, concrete dimensions, reinforcement ratio, the angle between the shear reinforcing bars and interface plane, and roughness of the interfaces. However, the mechanical properties of both the concrete and reinforcement as well as the bond interface have a vital role in each of the strength prediction models. These existing prediction models have been developed based on a wide range of experimental data with varying properties of concrete and reinforcements. In the composite specimens of ILC550 and HSC C100, properties of both the concrete as well as the use of fiber reinforcements for improving bond strengths are different from the widely used composite

specimens. The density and compressive strength of ILC (550 g/cm³) are significantly lower than the widely used lightweight concretes. In addition, the difference in predicted and experimental values of the FRP reinforced sample is much higher than the differences of the un-strengthened sample because the strength of FRPs is also higher than normal steel reinforcement. The tensile strength of FRPs was not exhausted in any of the shear bond strength tests, rather the shear bond failure of all the reinforced specimens occurred due to the crushing of ILC. Therefore, failure of reinforced specimens occurred at much higher values than those predicted by prediction models and this failure depends on the compressive strength of ILC.

Table 7 Experimental and predicted bond shear strength comparison

τ_b (MPa)	ILC-HSC	ILC-HSC with CFRP-25	ILC-HSC with CFRP-38	ILC-HSC with GFRP-25	ILC-HSC with GFRP-38	MAD
Experimental	0.49	2.05	1.38	2.11	1.39	-
EN	0.13	1.30	1.30	1.30	1.30	0.418
ACI	0.27	1.18	0.95	1.20	0.96	0.572
AASHTO	0.52	0.88	0.88	0.88	0.88	0.688
CSA	0.19	1.10	1.00	1.10	1.02	0.602
AS	0.04	1.49	1.16	1.51	1.15	0.422

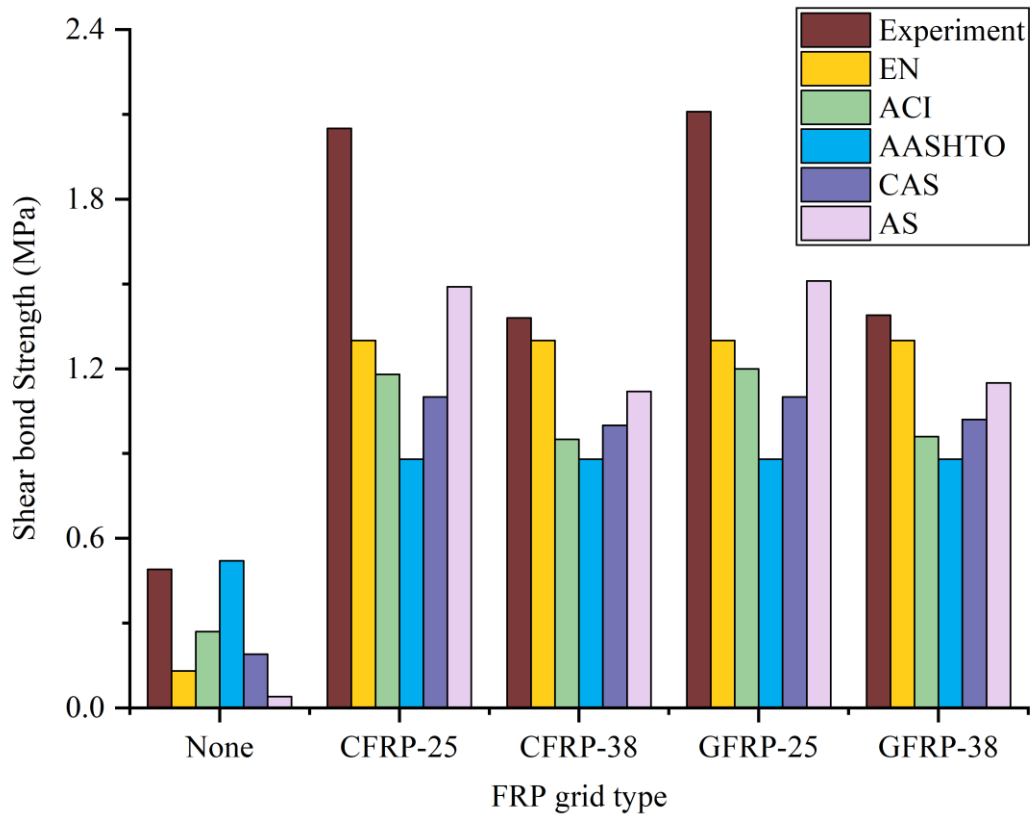


Figure 12 Comparison of experimental and predicted shear bond strengths

4.1.3 Developed shear bond strength prediction model

Comparison of experimental shear bond strength with five commonly used shear strength prediction models (Table 7) has revealed that all of the prediction models under-estimate this shear bond strength except for the AASHTO prediction model for the un-strengthened model. Since all the existing prediction models are based on the properties of NC and yielding of steel reinforcement, therefore, they cannot yield accurate results for normal and FRP reinforced ILC-HSC specimens. The strength of ILC is considerably lower than that of NC and FRP reinforcements do not yield as compared to steel reinforcement, therefore, the existing prediction models are not suitable for FRP reinforced ILC-HSC walls.

This strength prediction is crucial for strength and durability assessment of structures. Therefore, a new prediction model has been developed for ILC-HSC shear bond strength calculation. Since the predictions of the EN model were closest to experimental results with a mean absolute deviation (MAD) of 0.418, therefore, this model has been modified for the ILC-HSC specimen. Shear bond strength (τ_b) calculation formula of Eurocode-2 (Eq. 3.) has been modified according to the failure mechanism encountered in the shear bond strength tests (Figure 8). As yielding of the FRP reinforcement was not encountered in the experimental program, and all the reinforced specimens failed by crushing of the ILC, therefore, the prediction models have been based on the compressive strength of ILC instead of the yield strength of reinforcement. The shear bond strength prediction model has been developed through the simple linear regression analysis which is a linear approach to model the relationship between a dependent variable and one independent variable. For the shear bond strength, the dependent variable is the shear bond strength (τ_b), whereas the independent variable is the shear reinforcement ratio (ρ). The linear regression model has been fitted using the least-squares approach. The shear bond strength (τ_b) of un-strengthened and FRP reinforced ILC-HSC specimen can be calculated using Eq. 8.

$$\tau_b = \beta c f_{ct,ILC} + \varphi \rho f_{c,ILC} (\mu \sin \alpha + \cos \alpha) \quad (8)$$

Where β and φ are newly introduced parameters based on regression analysis to account for ILC, $f_{ct,ILC}$ and $f_{c,ILC}$ are the tensile and compressive strengths of ILC respectively and all the other parameters are the same as in Section 4.1.1. Taking ρ as the independent variable and τ_b as a dependent variable in the regression analysis (Figure 13), optimal values for β and φ are 3.023 and 120.431, respectively. These values of β and φ are based on a total of 5 values, obtained as an

average of 3 tests on 5 types of samples. The correlation coefficient R of 0.97 indicates the highest level of accuracy of regression analysis.

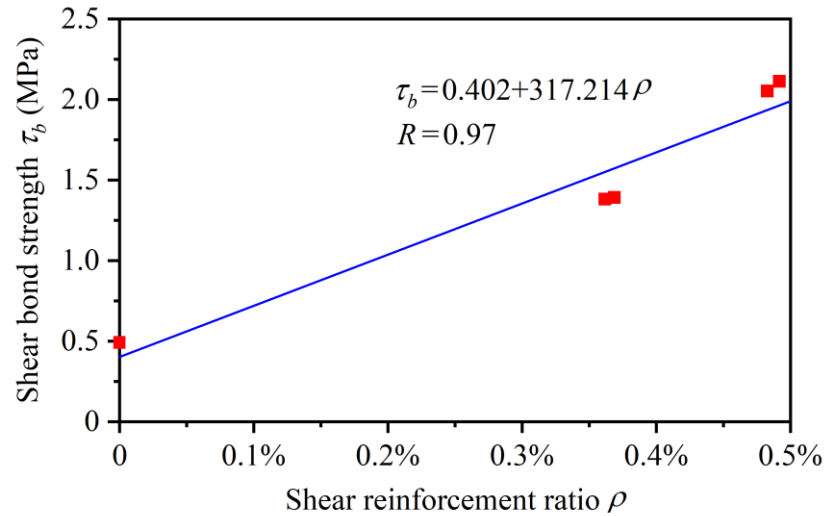


Figure 13 Linear regression of ρ and τ_b

To verify the accuracy of the developed shear bond strength prediction model, experimental results have been compared with those calculated using Eq. 8 with f_{ct} of 0.38 MPa, f_c of 4.39 MPa, α of 90° and shear reinforcement ratio ρ of 0%, 0.483%, 0.362%, 0.492%, and 0.369% for un-strengthened ILC-HSC, ILC-HSC reinforced with CFRP-25, CFRP-38, GFRP-25 and GFRP-38 respectively. Calculated results and their comparison with experimental values are presented in Table 8. This comparison shows that the developed prediction model can accurately calculate the shear bond strength of both the un-strengthened and FRP reinforced ILC-HSC specimens with a mean absolute deviation of just 0.142. A comparison of the developed prediction model with five commonly used models (Figure 14) also shows its accuracy for ILC-HSC specimens.

Table 8 Comparison of experimental shear bond strength with the developed prediction model

τ_b (MPa)	ILC-HSC	ILC-HSC with CFRP-25	ILC-HSC with CFRP-38	ILC-HSC with GFRP-25	ILC-HSC with GFRP-38	MAD
Experimental	0.49	2.05	1.38	2.11	1.39	-
Present study-Eq. (8)	0.40	1.93	1.55	1.96	1.57	0.142

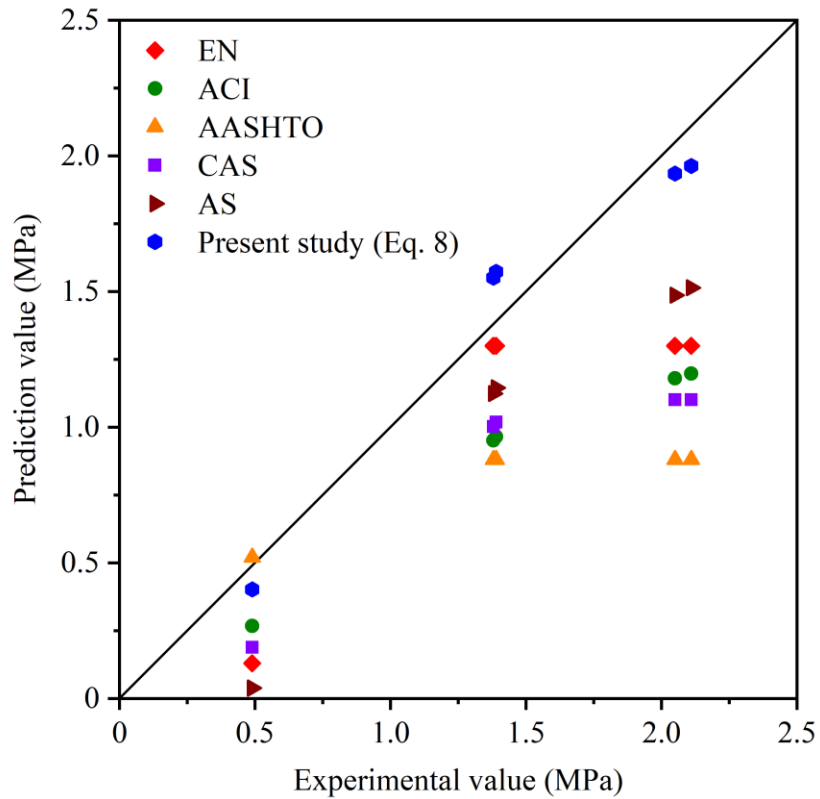


Figure 14 Comparison of the developed shear strength prediction model with commonly used prediction models

4.2 Developed prediction model for tensile bond strength

There are no codified tensile bond strength prediction models and there are very few studies that discuss the tensile bond strength prediction. In this research program, tensile bond strength prediction models have also been developed for ILC-HSC specimens based on their failure modes.

Unlike shear bond strength prediction, there is no existing formula for tensile strength on which the tensile shear bond strength equation could be based. The tensile bond strength prediction model has also been obtained using linear regression analysis in which the linear regression model is fitted using the least square approach. The tensile bond strength (f_{bt}) between ILC and HSC materials can be calculated using newly developed Eq. 9.

$$f_{bt} = \gamma c f_{ct,ILC} + \eta \kappa f_{ct,HSC} \quad (9)$$

Where γ and η are the factors for ILC and HSC respectively obtained through regression analysis of test data, c is a cohesion factor to account for the roughness of the bonded interface as per BS EN 1992-1-1: 2004 [34], $f_{ct,ILC}$ is the tensile strength of ILC, κ is the plane area ratio of FRP reinforcement to concrete and $f_{ct,HSC}$ is the tensile strength of HSC. Optimal values of γ and η obtained through regression analysis are 1.128 and 0.167, respectively. Similar to shear bond strength prediction models, these values are based on 5 average values of 15 test samples. The correlation coefficient R for this analysis is 1.00, which shows the high accuracy of regression (Figure 15).

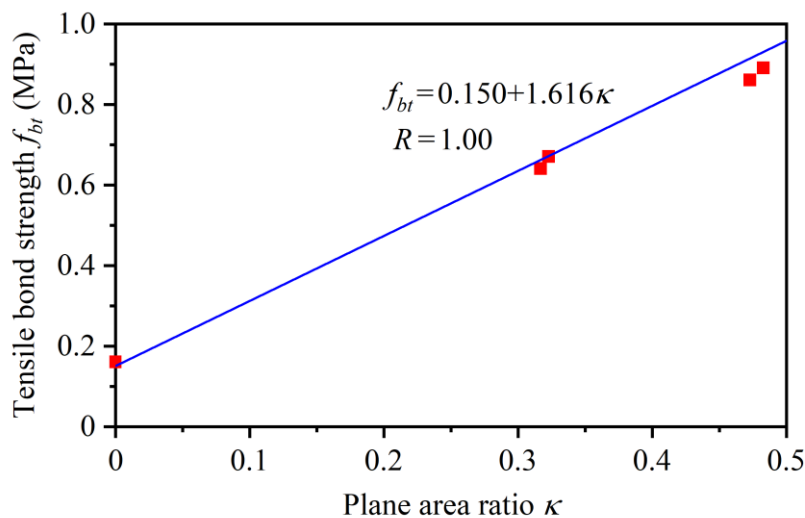


Figure 15 Linear regression of κ and f_{bt}

The accuracy of the developed tensile strength prediction model has also been assessed through comparison with experimental results. Values used for calculation of tensile bond strength using Eq. 9 are 1.128 for γ , 0.35 for c (smooth surface as per BS EN 1992-1-1: 2004 [34]), 0.38 MPa for $f_{ct,ILC}$, 0.167 for η and 9.67 MPa for $f_{ct,HSC}$. Plane area ratios (κ) are 0, 0.436, 0.320, 0.445, and 0.326 for un-strengthened ILC-HSC, ILC-HSC reinforced with CFRP-25, CFRP-38, GFRP-25 and GFRP-38 respectively. Calculation results and their comparison with experimental values are presented in Table 9 and Figure 16. Predicted values and MAD of 0.016 indicate that the developed equation for tensile bond strength (Eq. 9) is very accurate and can be utilized for un-strengthened and FRP reinforced ILC-HSC specimens.

Table 9 Comparison of experimental shear bond strength with the developed prediction model

f_{bt} (MPa)	ILC-HSC	ILC-HSC with CFRP-25	ILC-HSC with CFRP-38	ILC-HSC with GFRP-25	ILC-HSC with GFRP-38	MAD
Experimental	0.16	0.86	0.64	0.89	0.67	-
Present study-Eq. (9)	0.15	0.85	0.67	0.87	0.68	0.016

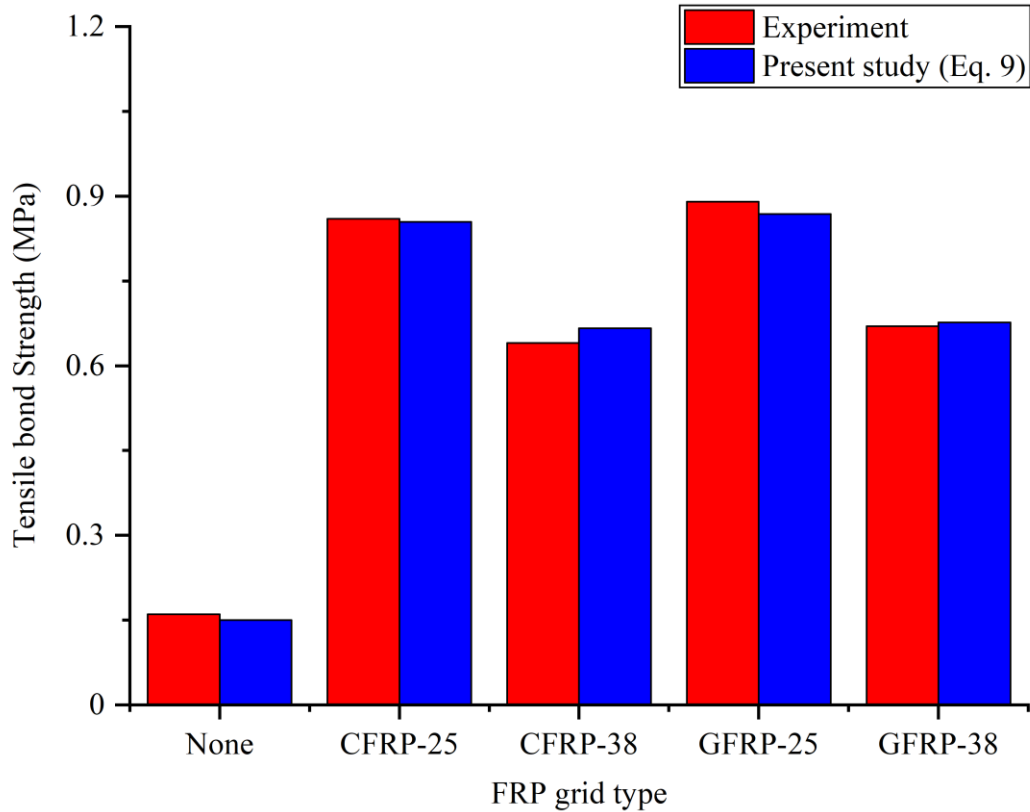


Figure 16 Comparison between experimental and prediction tensile bond strength (f_{bt})

5 Conclusions

The structural performance of infra-lightweight concrete having a dry density of 550 g/cm^3 (ILC550) has been improved by a 1 cm thick layer of high strength concrete with compressive strength of 103.32 MPa (HSC C100) on each side of ILC. As the performance of composite structures depends on the bond between them, therefore, an extensive study has been performed to assess the ILC-HSC bond strength under shear and tensile stresses. Also, bond strength has been improved using carbon and glass fiber reinforced polymers with two different grid arrangements i.e. 25 mm and 38 mm, and have been named FRP-25 and FRP-38 respectively. Moreover, the new prediction models have been developed to evaluate the shear and tensile bond strengths of

both the un-strengthened and FRP grid reinforced ILC-HSC structures. The following conclusions have been drawn from experimental and theoretical studies:

- The interface of the ILC-HSC composite specimen is the weakest part as both the shear and tensile bond strengths of ILC-HSC specimens are lower than the strength of ILC550, which is the weakest material in the specimen. Shear and tensile strengths of ILC550 are 0.52 MPa and 0.38 MPa respectively, whereas shear and tensile bond strengths of ILC-HSC composite specimen are 0.49 MPa and 0.16 MPa, respectively.
- Both the shear and tensile bond strengths are significantly improved using FRPs grid reinforcement. For shear bond strength, CFRP-25, CFRP-38, GFRP-25, and GFRP-38 with shear reinforcement ratios of 0.483%, 0.362%, 0.492%, and 0.369% respectively increased the shear bond strengths by 318%, 182%, 331% and 184%. For tensile bond strength, the tensile bond reinforcement ratios of 0.436, 0.320, 0.445, and 0.326 of CFRP-25, CFRP-38, GFRP-25, and GFRP-38 grids increased the tensile bond strengths by 438%, 300%, 456% and 319%.
- The increase in bond strength depends on the FRP reinforcement ratio i.e. reinforcement crossing the interface for shear bond strength and planar reinforcement in the loaded face for tensile bond strength, irrespective of the type of FRP. GFRP-25 with maximum reinforcement ratios of 0.492% and 0.445 in shear and tensile bonds increased the respective strengths by 331% and 456%.
- Comparison of experimental shear bond strength results of both the un-strengthened and strengthened ILC-HSC specimens with five commonly used shear bond strength prediction models i.e. EN model, ACI mode, AASHTO model, CSA model, and AS model has revealed that none of these models can be used to accurately predict the shear bond strength

of ILC-HSC specimens. Therefore, a new shear strength prediction model has been developed based on the EN model to account for the presence of ILC and FRP reinforcement. The developed shear strength prediction model is found to be accurate after comparing the predicted results with the experimental results and it can be utilized for both the un-strengthened and FRP reinforced ILC-HSC composite specimens.

- A new tensile bond strength model has been developed as currently there is no such model available. Comparison of experimental results with the developed tensile bond strength prediction model results has shown that the developed tensile bond strength prediction model can be used for accurate tensile bond strength prediction of both the un-strengthened and FRP reinforced ILC-HSC composite specimens.

As the bond strength prediction models are developed based on the properties and failure mechanisms of the overlay, substrate, and reinforcements, therefore, the developed prediction models are only applicable to the present study as it is the first study on FRP reinforced ILC-HSC walls. However, the accuracy of developed models will be verified by the authors in their future studies as well as researchers and designers of FRP reinforced HSC-ILC walls.

Acknowledgment:

The authors gratefully acknowledge the financial support provided by the Bundesministerium für Bildung und Forschung, German project (03ZZ03050), and the National Natural Science Foundation of China Youth Science Foundation Project (NSFC 51908012).

References:

- [1] M. Farzad, M. Shafieifar, A. Azizinamini, Experimental and numerical study on bond strength between conventional concrete and Ultra High-Performance Concrete (UHPC),

- Eng. Struct. 186 (2019) 297–305.
- [2] B.A. Tayeh, B.H. Abu Bakar, M.A. Megat Johari, Y.L. Voo, Mechanical and permeability properties of the interface between normal concrete substrate and ultra high performance fiber concrete overlay, *Constr. Build. Mater.* 36 (2012) 538–548. <https://doi.org/10.1016/j.conbuildmat.2012.06.013>.
- [3] B. Wang, S. Xu, F. Liu, Evaluation of tensile bonding strength between UHTCC repair materials and concrete substrate, *Constr. Build. Mater.* 112 (2016) 595–606.
- [4] I. De la Varga, Z.B. Haber, B.A. Graybeal, Enhancing shrinkage properties and bond performance of prefabricated bridge deck connection grouts: material and component testing, *J. Mater. Civ. Eng.* 30 (2018) 4018053.
- [5] P. Santos, E.N.B.S. Júlio, Interface Shear Transfer on Composite Concrete Members., *ACI Struct. J.* 111 (2014).
- [6] N. Randl, Design recommendations for interface shear transfer in fib Model Code 2010, *Struct. Concr.* 14 (2013) 230–241.
- [7] P. Dybeł, D. Wałach, Evaluation of the Development of Bond Strength between Two Concrete Layers, in: *IOP Conf. Ser. Mater. Sci. Eng.*, 2017. <https://doi.org/10.1088/1757-899X/245/3/032056>.
- [8] L. Hussein, L. Amleh, Structural behavior of ultra-high performance fiber reinforced concrete-normal strength concrete or high strength concrete composite members, *Constr. Build. Mater.* 93 (2015) 1105–1116.
- [9] K.N. Rahal, A.L. Khaleefi, A. Al-Sanee, An experimental investigation of shear-transfer strength of normal and high strength self compacting concrete, *Eng. Struct.* 109 (2016) 16–

25.

- [10] A.M. Diab, A.E.M.A. Elmoaty, M.R.T. Eldin, Slant shear bond strength between self compacting concrete and old concrete, *Constr. Build. Mater.* 130 (2017) 73–82.
- [11] P.M.D. Santos, E.N.B.S. Julio, Correlation between concrete-to-concrete bond strength and the roughness of the substrate surface, *Constr. Build. Mater.* 21 (2007) 1688–1695.
- [12] M.A. Yazdi, E. Dejager, M. Debraekeleer, E. Gruyaert, K. Van Tittelboom, N. De Belie, Bond strength between concrete and repair mortar and its relation with concrete removal techniques and substrate composition, *Constr. Build. Mater.* 230 (2020). <https://doi.org/10.1016/j.conbuildmat.2019.116900>.
- [13] M.A. Carbonell Muñoz, D.K. Harris, T.M. Ahlborn, D.C. Froster, Bond performance between ultrahigh-performance concrete and normal-strength concrete, *J. Mater. Civ. Eng.* 26 (2014) 1–9. [https://doi.org/10.1061/\(ASCE\)MT.1943-5533.0000890](https://doi.org/10.1061/(ASCE)MT.1943-5533.0000890).
- [14] G.F. Huseien, J. Mirza, M. Ismail, S.K. Ghoshal, A.A. Hussein, Geopolymer mortars as sustainable repair material: A comprehensive review, *Renew. Sustain. Energy Rev.* 80 (2017) 54–74.
- [15] M.A. Moeini, M. Bagheri, A. Joshaghani, A.A. Ramezani pour, F. Moodi, Feasibility of alkali-activated slag paste as injection material for rehabilitation of concrete structures, *J. Mater. Civ. Eng.* 30 (2018) 4018252.
- [16] Y. Zhang, P. Zhu, Z. Liao, L. Wang, Interfacial bond properties between normal strength concrete substrate and ultra-high performance concrete as a repair material, *Constr. Build. Mater.* 235 (2020). <https://doi.org/10.1016/j.conbuildmat.2019.117431>.
- [17] E. Brühwiler, E. Denarié, Rehabilitation and strengthening of concrete structures using

- ultra-high performance fibre reinforced concrete, *Struct. Eng. Int.* 23 (2013) 450–457.
- [18] A.A. Semendary, D. Svecova, Factors affecting bond between precast concrete and cast in place ultra high performance concrete (UHPC), *Eng. Struct.* 216 (2020). <https://doi.org/10.1016/j.engstruct.2020.110746>.
- [19] I. Rozsypalova, P. Danek, O. Karel, The bond strength by pull-off and direct tensile strength of concrete damaged by elevated temperatures, *IOP Conf. Ser. Mater. Sci. Eng.* 385 (2018). <https://doi.org/10.1088/1757-899X/385/1/012047>.
- [20] C. Zanotti, N. Randl, Are concrete-concrete bond tests comparable?, *Cem. Concr. Compos.* 99 (2019) 80–88. <https://doi.org/10.1016/j.cemconcomp.2019.02.012>.
- [21] Y. Ju, T. Shen, D. Wang, Bonding behavior between reactive powder concrete and normal strength concrete, *Constr. Build. Mater.* 242 (2020). <https://doi.org/10.1016/j.conbuildmat.2020.118024>.
- [22] A. Hückler, M. Schlaich, Structural Behavior of Reinforced Infra-Lightweight Concrete (ILC), *ACI Struct. J.* 116 (2019) 3–14.
- [23] BS-EN-206, Concrete-Specification, performance, production and conformity, 2014.
- [24] M. Schlaich, A. Hückler, *Infraleichtbeton* 2.0, 2012. <https://doi.org/10.1002/best.201200033>.
- [25] C. Lösch, P. Rieseberg, *Infraleichtbeton: Entwurf, Konstruktion, Bau*, in: M. Schlaich, R. Leibinger (Eds.), Fraunhofer IRB Verlag, 2018.
- [26] M. Schlaich, A. Hückler, *Infraleichtbeton: Reif für die Praxis, Beton-und Stahlbetonbau.* 112 (2017) 772–783.

- [27] Y. Liu, T. Tafsirojjaman, A.U.R. Dogar, A. Hückler, Shrinkage behavior enhancement of infra-lightweight concrete through FRP grid reinforcement and development of their shrinkage prediction models, *Constr. Build. Mater.* 258 (2020) 119649. <https://doi.org/10.1016/j.conbuildmat.2020.119649>.
- [28] J.M. Lees, A.U. Winistörfer, U. Meier, External prestressed carbon fiber-reinforced polymer straps for shear enhancement of concrete, *J. Compos. Constr.* 6 (2002) 249–256.
- [29] L. Dvorkin, O. Dvorkin, *Basics of Concrete Science*, St. Petersburg (Russia), 2006.
- [30] T. Tafsirojjaman, S. Fawzia, D. Thambiratnam, X. Zhao, Numerical investigation of CFRP strengthened RHS members under cyclic loading, *Structures.* 24 (2020) 610–626. <https://doi.org/10.1016/j.istruc.2020.01.041>.
- [31] T. Tafsirojjaman, S. Fawzia, D. Thambiratnam, X.L. Zhao, Seismic strengthening of rigid steel frame with CFRP, *Arch. Civ. Mech. Eng.* 19 (2019) 334–347. <https://doi.org/10.1016/j.acme.2018.08.007>.
- [32] Tafsirojjaman, S. Fawzia, D. Thambiratnam, Enhancement Of Seismic Performance Of Steel Frame Through CFRP Strengthening, *Procedia Manuf.* 30 (2019) 239–246. <https://doi.org/10.1016/j.promfg.2019.02.035>.
- [33] T. Tafsirojjaman, S. Fawzia, D. Thambiratnam, X.L. Zhao, Behaviour of CFRP strengthened CHS members under monotonic and cyclic loading, *Compos. Struct.* 220 (2019) 592–601. <https://doi.org/10.1016/j.compstruct.2019.04.029>.
- [34] BS-EN-1992-1-1:2004, Eurocode 2, Design of concrete structures-Part 1-1: General rules and rules for buildings, (2004).
- [35] American Concrete Institute, 318M–08: Building Code Requirements for Reinforced

- Concrete and Commentary, (2008) 473.
- [36] AASHTO LRFD, AASHTO LRFD bridge design specifications, Am. Assoc. State Highw. Transp. Off. Washington, DC. (2012).
- [37] Canadian Standards Association, Design of concrete structures, Mississauga, Ont.: Canadian Standards Association, 2004.
- [38] Australia Standards, AS 3600-2018: Concrete Structures, (2018).
- [39] British Standards Institution, BS EN 12390-7:2000 Part 7: Density of hardened concrete, 2000.
- [40] European Committee for Standardization (CEN), BS EN 206-1:2000 Concrete - Part 1: Specification, performance and conformity, 2000.
- [41] BS-EN-20, 12390-3: 2009, Test. Hardened Concr. Compressive Strength Test Specimens. (2009) 12390–12395.
- [42] E. Mörsch, Concrete-steel construction (der Eisenbetonbau), Engineering news publishing Company, 1909.
- [43] BS-EN-12390-13, Testing hardened concrete–Part 13: determination of secant modulus of elasticity in compression, Br. Stand. Inst. London, UK. (2013).
- [44] B.S. EN, BS EN 12667: 2001, Br. Stand. Inst. London, UK. (2001).
- [45] Cement Composition, Specifications and Conformity Criteria for Common Cements, in: BS EN 197-1, 2011: pp. 191–197.
- [46] ACI Committee 363, Report on High-Strength Concrete (ACI 363R-10), ACI, 2010.
- [47] BS-EN-1992-1-2, Eurocode 2: Design of Concrete Structures-Part 1-2: General Rules–

Structural Fire Design, (2004).

- [48] J.F. Berthet, I. Yurtdas, Y. Delmas, A. Li, Evaluation of the adhesion resistance between steel and concrete by push out test, *Int. J. Adhes. Adhes.* 31 (2011) 75–83. <https://doi.org/10.1016/j.ijadhadh.2010.11.004>.
- [49] European Standards, BS-EN 12090:2013 Thermal insulating products for building applications–Determination of shear behaviour, 2013.
- [50] FIB, Model Code 2010, 2011. <https://doi.org/10.1002/9783433604090.ch6>.
- [51] European Committee for Standardization (CEN), EN 1015-12: Methods of test for mortar for masonry–Part 12: Determination of adhesive strength of hardened rendering and plastering mortars on substrates, (2016).